

# Barium Carbonate Nanoparticles as Synergistic Catalysts for the Oxygen Reduction Reaction on $\text{La}_{0.6}\text{Sr}_{0.4}\text{Co}_{0.2}\text{Fe}_{0.8}\text{O}_{3-\delta}$ Solid-Oxide Fuel Cell Cathodes

Tao Hong,<sup>[a, b]</sup> Kyle S. Brinkman,<sup>[b]</sup> and Changrong Xia\*<sup>[a]</sup>

Barium carbonate ( $\text{BaCO}_3$ ) nanoparticles have been demonstrated to have excellent synergistic catalytic activity for the oxygen reduction reaction on  $\text{La}_{0.6}\text{Sr}_{0.4}\text{Co}_{0.2}\text{Fe}_{0.8}\text{O}_{3-\delta}$  (LSCF) and LSCF-SDC (SDC =  $\text{Sm}_{0.2}\text{Ce}_{0.8}\text{O}_{1.9}$ ), which are typical mixed conducting electrode materials for solid-oxide fuel cells (SOFCs). The  $\text{BaCO}_3$  nanoparticles were deposited into the porous electrodes through an infiltration/impregnation method with barium acetate as the precursor. Electrochemical impedance analysis indicated that  $\text{BaCO}_3$  dramatically reduced the resistance associated with the low-frequency response, which suggests that  $\text{BaCO}_3$  greatly enhances the kinetics of the surface reaction process. Electrical conductivity relaxation experiments

revealed that  $\text{BaCO}_3$  particles enlarged the oxygen chemical surface exchange coefficient by a factor of up to eight. As a result, the interfacial polarization resistance of both the LSCF and LSCF-SDC electrodes was greatly reduced, from 0.28 and 0.13 to 0.12 and 0.047  $\Omega\text{cm}^2$ , respectively, at 700 °C. In addition, the single-cell performance was also improved and demonstrated peak power density from 0.66 and 0.71 to 0.73 and 0.81  $\text{Wcm}^2$  for the LSCF and LSCF-SDC cathodes, respectively, at 700 °C. The LSCF electrode infiltrated with  $\text{BaCO}_3$  nanoparticles also exhibited higher stability than the bare LSCF electrode in tests conducted under typical SOFC conditions for over 340 h of operation.

## 1. Introduction

The perovskite oxide  $\text{La}_{0.6}\text{Sr}_{0.4}\text{Co}_{0.2}\text{Fe}_{0.8}\text{O}_{3-\delta}$  (LSCF) has been extensively investigated as a catalyst for the oxygen reduction reaction (ORR) in intermediate-temperature solid-oxide fuel cells (SOFCs) and membrane reactors for oxygen separation because of its good electrochemical catalytic activity and high ionic and electronic conductivity in the temperature range of 500 to 800 °C.<sup>[1,2]</sup> Furthermore, its oxygen catalytic activity was improved by the application of catalytically active nanoparticles through an infiltration method.<sup>[3–5]</sup> Initially, precious metals, such as Ag, Pd, and Rh, were used to infiltrate the LSCF surface to enhance the activity, that is, reduce the interfacial polarization resistance of the cathodes for SOFCs.<sup>[6–10]</sup> For example, at 600 °C, the infiltration of 1.2  $\text{mgcm}^{-2}$  Pd on a porous LSCF electrode reduced the resistance from 5.4 to 2.9  $\Omega\text{cm}^2$ .<sup>[8]</sup> Such an enhancement is caused by the unique properties of precious metals, such as Ag,<sup>[11]</sup> Pt,<sup>[12]</sup> and Pd,<sup>[13]</sup> which have historically demonstrated very good catalytic activity for ORR. However, cost has been a major concern for the commercialization of precious-metal-containing materials systems. In addition, their long-term stability is also a significant concern in high-temperature applications, such as in SOFCs.

In addition to precious-metal catalysts, the infiltration of oxides, such as doped ceria  $\text{Sm}_{0.2}\text{Ce}_{0.8}\text{O}_{2-\delta}$  (SDC)<sup>[14]</sup> and  $\text{Gd}_{0.1}\text{Ce}_{0.9}\text{O}_{2-\delta}$  (GDC),<sup>[8]</sup> have been reported to improve the ORR catalytic activity. Because doped ceria has a very high ionic conductivity, it was proposed that the improvement was mainly due to the enlarged three-phase boundaries (TPB) at which ORR principally occurs. Additionally, it was found that doped ceria could increase the surface oxygen exchange rate by a factor of up to 10, which suggests that the ORR is enhanced through a surface reaction rather than the bulk transport process.<sup>[15]</sup> In SOFC cathodes, the ORR is typically limited by the oxygen disassociation on the LSCF surface rather than the ionic transportation within the electrode bulk, which means that enhancing the surface reaction kinetics is even more effective than extending the three-phase boundary in these material systems.<sup>[15,16]</sup> For this reason, the application of  $\text{La}_{0.4875}\text{Ca}_{0.0125}\text{Ce}_{0.5}\text{O}_{2-\delta}$  (LCC) with very low ionic conductivity could also significantly enhance ORR activity on LSCF.<sup>[17]</sup>

ORR catalysts, such as  $\text{La}_{0.8}\text{Sr}_{0.2}\text{MnO}_{3-\delta}$  (LSM),<sup>[18]</sup>  $\text{Pr}_{0.8}\text{Sr}_{0.2}\text{MnO}_{3-\delta}$  (PSM),<sup>[19]</sup> and  $\text{Sm}_{0.5}\text{Sr}_{0.5}\text{CoO}_{3-\delta}$  (SSC),<sup>[20]</sup> have been investigated as infiltration phases to improve the surface reaction kinetics. These materials have all demonstrated very good ORR catalytic activity. The application of these materials in nanostructured form by using an infiltration method can effectively extend the active sites by increasing the surface area for ORR.

Recently, we reported that the application of  $\text{BaCO}_3$  nanoparticles demonstrate greater improvement in the ORR catalytic activity than precious metals.<sup>[21,22]</sup> Herein, we extend our investigations by examining the synergistic effect of  $\text{BaCO}_3$  nano-

[a] Dr. T. Hong, Dr. C. Xia  
Department of Materials Science and Engineering  
University of Science and Technology of China  
Hefei, Anhui 230026 (China)  
E-mail: xiacr@ustc.edu.cn

[b] Dr. T. Hong, Dr. K. S. Brinkman  
Department of Materials Science and Engineering  
Clemson University  
Clemson, SC 29634 (USA)

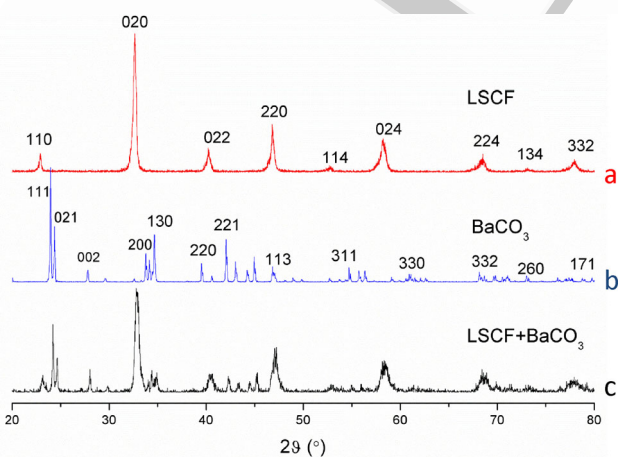
particles on the ORR activity of the LSCF catalyst. Electrical conductivity relaxation experiments revealed that  $\text{BaCO}_3$  greatly accelerated the oxygen incorporation process, which resulted in reduced interfacial polarization resistance of the LSCF electrode on a SDC electrolyte. The application of  $\text{BaCO}_3$  nanoparticles in a LSCF-SDC composite cathode also achieves excellent fuel-cell performance. Full-cell testing was employed to examine the durability and electrochemical performance of cathodes with and without  $\text{BaCO}_3$  under practical fuel-cell conditions and also to link the time-dependent surface structure changes to the observed electrochemical properties.

## 2. Results and Discussion

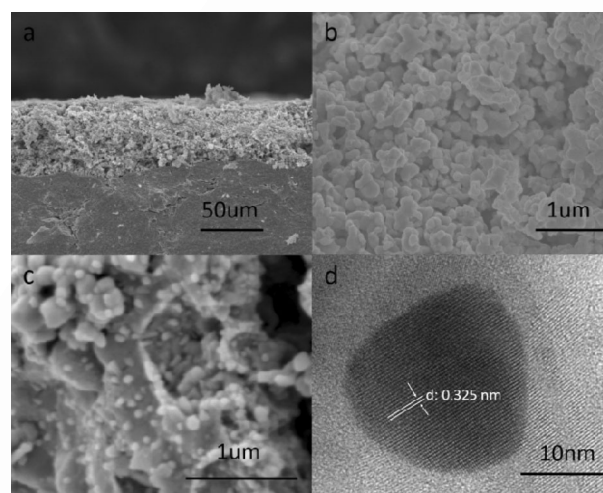
### 2.1. Formation of $\text{BaCO}_3$ Nanoparticles on the LSCF Surface

Figure 1 a shows the XRD pattern of a LSCF powder, which exhibits a perovskite structure. Figure 1 b is the pattern of a  $\text{BaCO}_3$  powder prepared by heating  $\text{Ba}(\text{Ac})_2$  at  $800^\circ\text{C}$  for 2 h.<sup>[22]</sup> Figure 1 c is the pattern for a composite powder, which is obtained by coheating a LSCF/ $\text{Ba}(\text{Ac})_2$  (weight ratio 5:5) mixture at  $800^\circ\text{C}$  for 10 h. All the diffraction peaks in Figure 1 c can be attributed to either LSCF or  $\text{BaCO}_3$ , which demonstrates that  $\text{Ba}(\text{Ac})_2$  decomposes to  $\text{BaCO}_3$  in the presence of LSCF. In addition,  $\text{BaCO}_3$  is chemically compatible with LSCF at  $800^\circ\text{C}$ .

Figure 2 shows the typical cross-sectional views of a LSCF electrode supported on a dense SDC electrolyte. Figure 2 a shows a representative view for the porous LSCF. The LSCF layer is about  $50\ \mu\text{m}$  thick. Figure 2 b indicates the LSCF grain size is in the range of 0.2 to  $0.3\ \mu\text{m}$ . The grain surfaces are very clean and smooth. In contrast, as suggested by Figure 2 c, after the infiltration treatment, a small amount of nanoscale discrete  $\text{BaCO}_3$  particles are uniformly deposited on the LSCF grain surface. The  $\text{BaCO}_3$  particle size is about 20 nm (Figure 2 d), which indicates an average  $d$ -spacing of 0.325 nm for the (002) planes of orthorhombic  $\text{BaCO}_3$ .



**Figure 1.** XRD patterns for a) LSCF powder heated at  $700^\circ\text{C}$  for 2 h, b)  $\text{Ba}(\text{Ac})_2$  powder heated at  $800^\circ\text{C}$  for 2 h, and c) LSCF +  $\text{Ba}(\text{Ac})_2$  powders heated at  $800^\circ\text{C}$  for 10 h.



**Figure 2.** Microstructure images for LSCF electrodes and  $\text{BaCO}_3$  nanoparticles. a, b) SEM images of a bare LSCF electrode supported on a dense SDC electrolyte, c) SEM image for a LSCF loaded with 9.2 wt%  $\text{BaCO}_3$  nanoparticles, d) TEM image of a nanosized  $\text{BaCO}_3$  particle.

### 2.2. Synergistic Catalytic Activity with LSCF Electrodes

Figure 3 summarizes the effect of  $\text{BaCO}_3$  loading on the area-specific interfacial polarization resistance (ASR), which is determined from the AC impedance spectra. The resistance goes through a substantial decrease after the porous LSCF electrode is infiltrated with  $\text{BaCO}_3$  nanoparticles. For example, at  $700^\circ\text{C}$ , the bare LSCF electrode exhibits an ASR of  $0.29\ \Omega\ \text{cm}^2$ . The resistance decreased to  $0.14\ \Omega\ \text{cm}^2$  when 5.1 wt%  $\text{BaCO}_3$  was infiltrated, and further to  $0.12\ \Omega\ \text{cm}^2$  at a  $\text{BaCO}_3$  loading of 9.2 wt%. However, further increases in the  $\text{BaCO}_3$  loading resulted in a slightly increase in the electrode resistance to 0.15 and  $0.16\ \Omega\ \text{cm}^2$  at 12.4 and 13.5 wt%, respectively.

Given that  $\text{BaCO}_3$  does not have any catalytic activity on the ORR, the reduced resistance must be caused by a synergistic

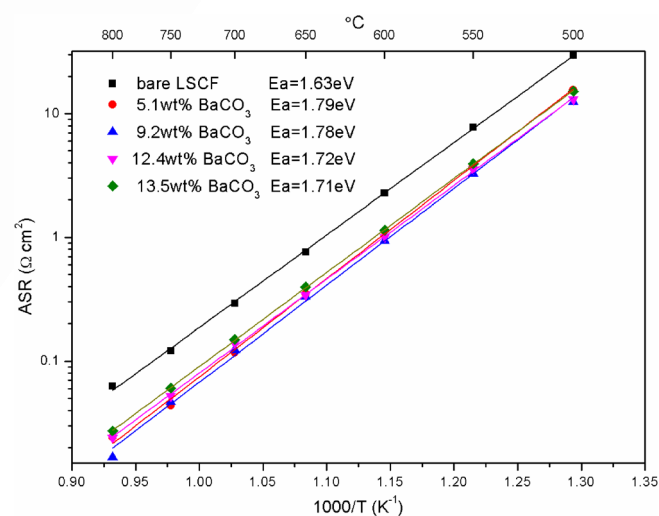


**Figure 3.** The Arrhenius relationship between area-specific interfacial polarization resistance (ASR) and temperature for LSCF electrodes infiltrated with different loadings of  $\text{BaCO}_3$ .

effect on the electrochemical reaction. The synergistic catalytic activity is significant because the resistance at 700 °C is even lower than those infiltrated with Pd, Rh, and SDC when the same electrolyte is applied. Table 1 gives the data for LSCF electrodes infiltrated with various materials reported in the literature. The electrode polarization resistance depends not only on the electrocatalyst activity but also on the microstructures of electrolyte and the electrode. Thus, direct comparison on the electrode resistance does not fully show the infiltration effect of different materials because their microstructures could be different as a result of being prepared by different processes and by various groups. The infiltration effect is compared by using the performance-improving factor ( $f_p$ ), which was proposed by Jiang<sup>[5]</sup> to describe the enhancement in the catalytic activity of the electrode materials. For our samples, the improvement factor from 500 to 800 °C was between 2.28

and 3.74 when 9.2 wt% infiltrated BaCO<sub>3</sub> was used as a catalyst. These values are comparable with those reported for precious metals, such as Pd, Ag, and Rh, which are believed to be excellent catalysts for ORR. It is also comparable to those reported for doped ceria, which is known to be an excellent ionic conductor and improves the ORR by extending the TPB length. In addition, it is comparable to those measured for typical mixed conductors, which are high-temperature electrocatalysts for ORR. In fact, the  $f_p$  of BaCO<sub>3</sub> is higher than the most of the materials listed in Table 1. This high improvement factor suggests that BaCO<sub>3</sub> is an excellent synergistic catalyst for ORR, considering the fact that it is apparently functioning neither as a catalyst nor as an ionic-electronic conductor.

**Table 1.** The performance of LSCF electrodes infiltrated with various materials.

| Infiltrated material   | Electrolyte | Coating type      | Performance   | $f_p$ | Ref.            |
|--|-------------|-------------------|---|-------|-----------------|
| Pd (7.5 $\mu\text{g cm}^{-2}$ )  | GDC         | discrete particle | 700 °C ASR<br>infiltrated: 0.04 $\Omega\text{ cm}^2$<br>bare: 0.14 $\Omega\text{ cm}^2$         | 3.5   | [6]             |
| Pd (1.2 $\text{mg cm}^{-2}$ )  | GDC         | discrete particle | 600 °C ASR<br>infiltrated: 2.9 $\Omega\text{ cm}^2$<br>bare: 5.4 $\Omega\text{ cm}^2$           | 1.86  | [8]             |
| Pd   | SDC         | discrete particle | 700 °C ASR<br>infiltrated: 0.247 $\Omega\text{ cm}^2$<br>bare: 0.35 $\Omega\text{ cm}^2$        | 1.42  | [9]             |
| Ag (18 wt%)  | SDC         | discrete particle | 530 °C power density<br>infiltrated: 0.42 $\text{W cm}^{-2}$<br>bare: 0.32 $\text{W cm}^{-2}$   | 1.31  | [7]             |
| Rh   | SDC         | discrete particle | 700 °C ASR<br>infiltrated: 0.261 $\Omega\text{ cm}^2$<br>bare: 0.35 $\Omega\text{ cm}^2$        | 1.34  | [9]             |
| Ag (18 wt%)  | YSZ         | discrete particle | 630 °C power density<br>infiltrated: 0.25 $\text{W cm}^{-2}$<br>bare: 0.16 $\text{W cm}^{-2}$   | 1.56  | [7]             |
| BaCO <sub>3</sub> (9.2 wt%)  | SDC         | discrete particle | 700 °C ASR<br>infiltrated: 0.29 $\Omega\text{ cm}^2$<br>bare: 0.12 $\Omega\text{ cm}^2$         | 2.37  | this work ■ ? ■ |
| BaCO <sub>3</sub> (9.2 wt%)  | SDC         | discrete particle | 600 °C ASR<br>infiltrated: 0.94 $\Omega\text{ cm}^2$<br>bare: 2.27 $\Omega\text{ cm}^2$         | 2.42  | this work ■ ? ■ |
| SDC  | SDC         | discrete particle | 700 °C ASR<br>infiltrated: 0.17 $\Omega\text{ cm}^2$<br>bare: 0.4 $\Omega\text{ cm}^2$          | 2.35  | [14]            |
| GDC (1.5 $\text{mg cm}^{-2}$ )   | GDC         | discrete particle | 600 °C ASR<br>infiltrated: 1.6 $\Omega\text{ cm}^2$<br>bare: 5.4 $\Omega\text{ cm}^2$           | 3.38  | [8]             |
| LCC  | SDC         | discrete particle | 750 °C ASR<br>infiltrated: 0.184 $\Omega\text{ cm}^2$<br>bare: 0.3 $\Omega\text{ cm}^2$         | 1.63  | [23]            |
| SSC  | SDC         | discrete particle | 650 °C ASR<br>infiltrated: 0.12 $\Omega\text{ cm}^2$<br>bare: 0.42 $\Omega\text{ cm}^2$         | 3.5   | [19]            |
| LSM  | SDC         | continuous film   | 700 °C power density<br>infiltrated: 0.655 $\text{W cm}^{-2}$<br>bare: 0.549 $\text{W cm}^{-2}$ | 1.19  | [17]            |
| Pr <sub>1-x</sub> Sr <sub>x</sub> MnO <sub>3-<math>\delta</math></sub> | SDC         | continuous film   | 750 °C ASR<br>infiltrated: 0.107 $\Omega\text{ cm}^2$<br>bare: 0.126 $\Omega\text{ cm}^2$       | 1.18  | [18]            |
| PrSrCoMnO <sub>6</sub>   | SDC         | continuous film   | 750 °C ASR<br>infiltrated: 0.093 $\Omega\text{ cm}^2$<br>bare: 0.126 $\Omega\text{ cm}^2$       | 1.35  | [18]            |

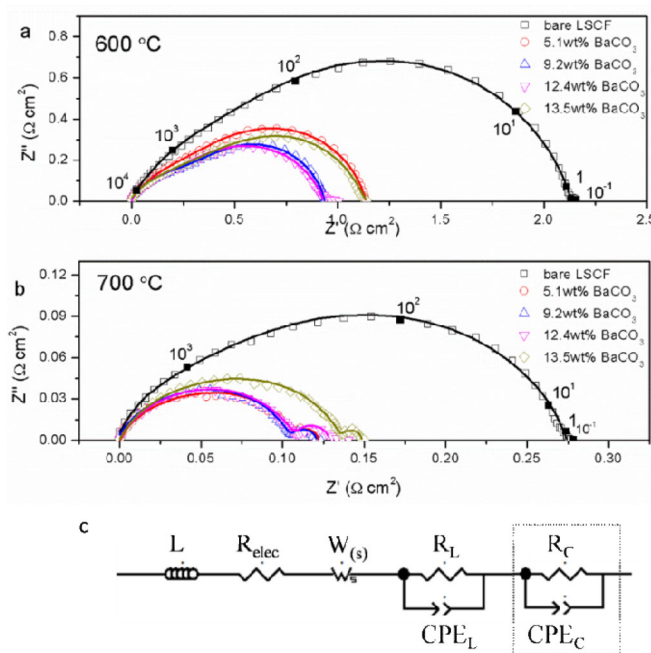


**Figure 4.** Impedance spectra at a) 600 and b) 700 °C for LSCF electrodes infiltrated with various amounts of BaCO<sub>3</sub>, and c) the fitting circuit. The typical frequency number and fitting results (the lines) are shown on the spectra.

### 2.3. BaCO<sub>3</sub> Effect on the Impedance Spectrum

Figure 4 shows the typical impedance spectra for the symmetric cells. The electrode reaction processes of porous LSCF cathodes on doped ceria electrolytes have been carefully investigated by Grunbaum et al.<sup>[27]</sup> by using electrochemical impedance spectroscopy. By changing oxygen partial pressure from 10<sup>-4</sup> to 0.02 atm, they have proposed an electrical equivalent circuit (Figure 4c). It consists of a pure inductance ( $L$ ) connected in series with a pure resistive element,  $R_{elec}$  which represents the electrolyte resistance, a high-frequency Warburg impedance ( $W$ ), and a circuit element consisting of a resistance ( $R_L$ ) in parallel with a constant-phase element ( $CPE_L$ ). The last combination ( $R_L$ - $CPE_L$ ) is used to fit the low-frequency range of the impedance diagram. The two-arc fitting lines match well with the experimental results (Figures 4a and 4b). The effect of BaCO<sub>3</sub> infiltration is clearly demonstrated by a reduction in the width between the high- and low-frequency intercepts in the spectra. It should be noted that at 700 °C, the arc labeled  $R_C$ - $CPE_C$  for concentration polarization was observed for the electrodes infiltrated with BaCO<sub>3</sub>. For the bare LSCF, the arc was not observed. When BaCO<sub>3</sub> particles were deposited the electrode porosity was reduced, which could cause the observed concentration-polarization effects.

Figure 5 shows the loading effect on  $R_W$  and  $R_L$  measured at 600 and 700 °C. The fitted values for the bare LSCF are consistent with our previous results.<sup>[28]</sup>  $R_W$  is almost independent of the loading, which demonstrates that the BaCO<sub>3</sub> nanoparticles do not have any obvious effects on the process associated with the high-frequency response. Compared with that of the bare LSCF electrode, the impedance loop that appears at low frequencies varies dramatically with the infiltration of BaCO<sub>3</sub>.

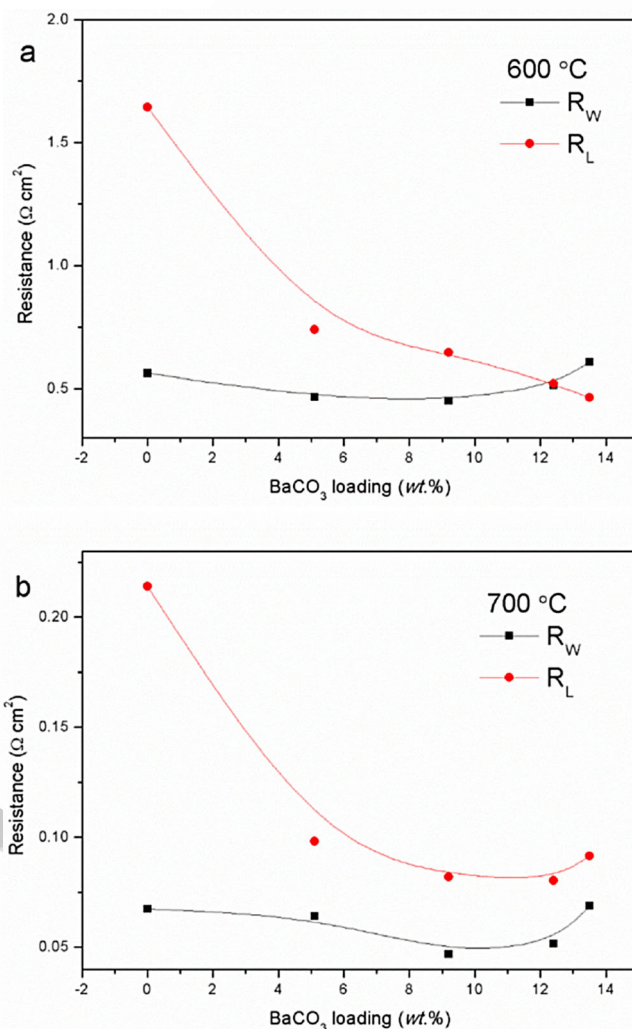


**Figure 5.**  $R_W$  and  $R_L$  at a) 600 and b) 700 °C obtained by fitting the experimental data based on the equivalent circuits shown in Figure 4.

For example, at 600 °C,  $R_L$  is 1.64  $\Omega \text{ cm}^2$  for the bare LSCF cathode. It decreases to 0.74  $\Omega \text{ cm}^2$  for the electrode with 5.1 wt% BaCO<sub>3</sub> and to 0.46  $\Omega \text{ cm}^2$  with 13.5 wt% BaCO<sub>3</sub>. According to the model suggested by Maier et al.<sup>[29,30]</sup> and Liu et al.<sup>[31]</sup> for the LSCF electrodes, the high-frequency feature can be assigned to the oxygen ion transfer across the interface between the cathode and the electrolyte, whereas the low-frequency response to the electrochemical oxygen surface exchange reaction. Thus, infiltration of BaCO<sub>3</sub> has a negligible effect on the oxygen ion transport transfer process but highly accelerates the surface reaction process, which causes the significant catalytic activity for ORR.

### 2.4. BaCO<sub>3</sub> Effect on the Oxygen Surface Exchange Coefficient

The BaCO<sub>3</sub> effect on the surface reaction properties was further investigated by using the electrical conductivity relaxation (ECR) method by comparing the relaxation profiles.<sup>[15]</sup> Figure 6 presents the typical microstructures of the

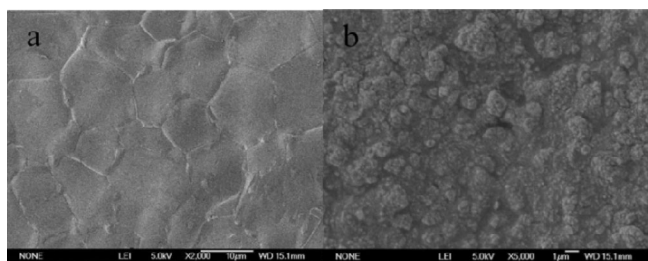


**Figure 6.** SEM images for the microstructures of a) the surface of a dense bare LSCF bar and b) the surface of a LSCF bar loaded with 0.85 mg cm<sup>-2</sup> BaCO<sub>3</sub>.

LSCF bars that were used for the ECR measurement. The bare LSCF bar was dense and consisted of grains about 10 μm in size, as depicted in Figure 6a. After dip-coating and firing, the bar surface was partially covered with 0.85 mg cm<sup>-2</sup> BaCO<sub>3</sub> particles (Figure 6b). The total LSCF surface area exposed to the gas phase was reduced by the BaCO<sub>3</sub> particles.

Figure 7a shows the normalized conductivity at 700 °C as a function of time for the LSCF bars with and without BaCO<sub>3</sub>.

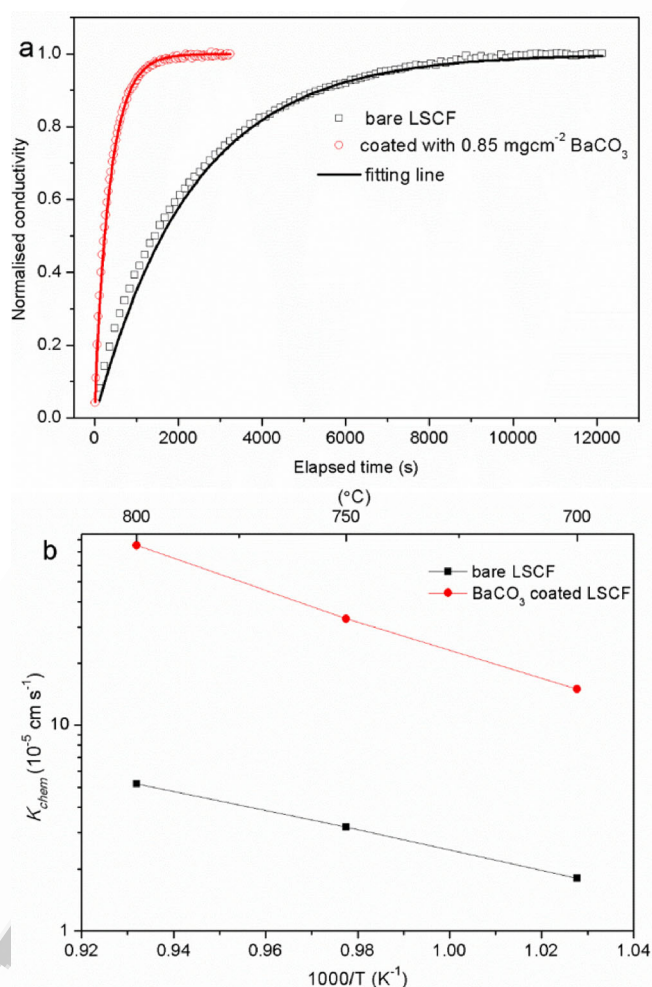


**Figure 7.** a) Relaxation profiles at 700 °C and b) chemical oxygen surface exchange coefficients for a bare LSCF bar and a LSCF bar coated with BaCO<sub>3</sub> particles.

The elapsed time to reach equilibrium was about 11 000 s for the bare LSCF bar. This was reduced to 2000 s when BaCO<sub>3</sub> was deposited, although the total LSCF surface area exposed to the gas phase was obviously reduced by the BaCO<sub>3</sub> particles. Because the bulk diffusion properties are exactly the same for the two bars, the reduced relaxation time must be attributed to an increase in the oxygen surface exchange process, which means an increase in the chemical surface exchange coefficient ( $K_{\text{chem}}$ ) measured from the ECR profiles.<sup>[32,33]</sup> Figure 7b compares the  $K_{\text{chem}}$  values obtained from ECR measurements at different temperatures. At 700 °C, the  $K_{\text{chem}}$  for the bare LSCF was  $1.8 \times 10^{-5} \text{ cm s}^{-1}$ , which is consistent with reported literature values for LSCF at the same temperature, from  $0.7$  to  $2.5 \times 10^{-5} \text{ cm s}^{-1}$ .<sup>[16,34,35]</sup> The variation in the literature  $K_{\text{chem}}$  values could be caused by differences in grain size and grain boundary lengths that result from various fabrication conditions. After the LSCF surface was covered with BaCO<sub>3</sub> particles, the measured  $K_{\text{chem}}$  value increased to  $15 \times 10^{-5} \text{ cm s}^{-1}$ , which is about eight times larger than the value for bare LSCF. For LSCF coated with BaCO<sub>3</sub> particles, oxygen exchange can occur through any routes that occur at the following sites: route I on the LSCF surface, that is, the LSCF–gas two phase interface; route II on the BaCO<sub>3</sub> surface, the BaCO<sub>3</sub>–gas; and route III at the three-phase interface of LSCF–BaCO<sub>3</sub>–gas. Coating BaCO<sub>3</sub> reduces the reaction rate associated with route I because the LSCF–gas area is reduced by the BaCO<sub>3</sub> particles. It should be noted that the contribution of route II is negligible because BaCO<sub>3</sub> is known as a non-electronic-ionic conductor that is not active for the oxygen incorporation reaction. Thus, the reduced relaxation time and the enhanced surface reaction rate should be caused only by route III, the reaction associated with both LSCF and BaCO<sub>3</sub>, which could result in an excellent synergistic ORR catalytic activity. However, further investigation is needed to reveal such effect. The ECR results also agree well with the electrochemistry impedance spectra; both measurements demonstrate a significant increase in the kinetics of the surface reaction process.

## 2.5. Synergistic Catalytic Activity with a LSCF-SDC Electrode

The synergistic catalytic effect was further demonstrated by using LSCF-SDC composite electrodes. Figure 8 shows the ASRs for the composite electrodes infiltrated with various amount of BaCO<sub>3</sub> particles. In comparison with the single-phase LSCF electrode (Figure 3), the bare LSCF-SDC composite showed much higher electrochemical performance. For example, the ASR at 600 °C was  $1.04 \Omega \text{ cm}^2$  for the composite whereas it was  $2.27 \Omega \text{ cm}^2$  for bare LSCF. The improvement in the electrochemical performance can be attributed to the fact that SDC has high ionic conductivity, which can extend the reaction sites, that is, TPBs, and enhance the surface reaction kinetics.<sup>[15]</sup> The resistance of the LSCF electrode infiltrated with 9.2 wt% BaCO<sub>3</sub> was found to be  $0.94 \Omega \text{ cm}^2$ , which was even lower than the LSCF-SDC composite electrode. The synergistic catalytic activity of BaCO<sub>3</sub> was observed to be greater than the improvement obtained by using an oxygen ion conductor composite, such as SDC.

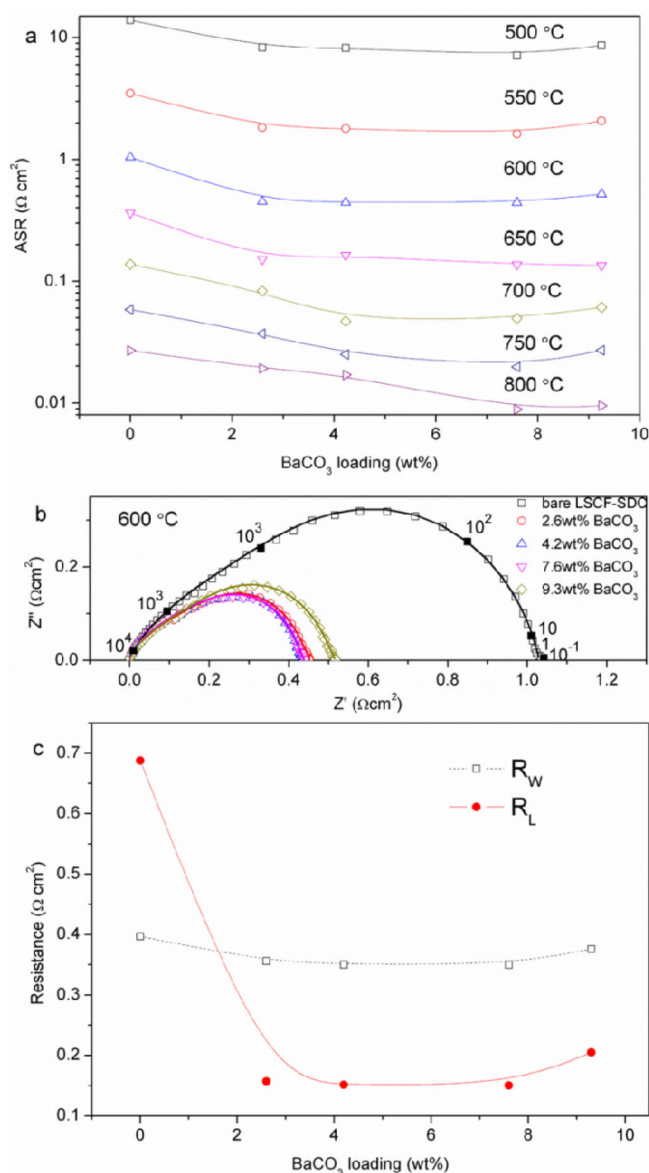


**Figure 8.** a) ASR measured at different temperatures for LSCF-SDC electrodes infiltrated with various amounts of BaCO<sub>3</sub>. b) Impedance spectra and c)  $R_w$  and  $R_L$  at 600 °C.

In the LSCF-SDC electrodes, infiltration of BaCO<sub>3</sub> reduces the electrode resistance over the entire testing temperature range used in these studies (Figure 8a). Even relatively low loadings, such as 2.59 wt% infiltrated BaCO<sub>3</sub>, decreased the resistance at 600 °C from 1.04 to 0.46 Ω cm<sup>2</sup>. The lowest resistance observed was 0.44 Ω cm<sup>2</sup>, achieved at a loading of 7.59 wt%. The average  $f_p$  was 2.56, which demonstrates significant synergistic catalytic activity for ORR in LSCF-SDC electrodes. Figure 8b shows the impedance spectra at 600 °C for LSCF-SDC electrodes with various BaCO<sub>3</sub> loadings. The impedance spectra were also analyzed by using the equivalent circuit shown in Figure 4c. Figure 8c shows the obtained  $R_w$  and  $R_L$  values. Similar to the results obtained with the LSCF electrodes,  $R_w$  remains almost the same whereas  $R_L$  was reduced in the presence of BaCO<sub>3</sub> nanoparticles. In the LSCF-SDC composite electrode, the SDC back-

bone provides the oxygen ion transport pathway and is not affected by the BaCO<sub>3</sub> particles on the surface. Significant reduction was observed for the low-frequency response,  $R_L$  exhibited a 78% decrease from 0.69 to 0.15 Ω cm<sup>2</sup> with 4.2 wt% BaCO<sub>3</sub>. The low-frequency response demonstrates that the synergistic effect in the composite electrode is also associated with the surface reaction process, which is believed to take place at the three-phase boundaries.

## 2.6. Single-Cell Performance

The synergistic catalytic activity was also demonstrated in single cells that consisted of Ni-YSZ anodes, YSZ electrolytes, and SDC interlayers with humidified hydrogen as the fuel and ambient air as the oxidant. Figure 9a shows the current–voltage characteristics and corresponding power density between 650 and 800 °C for anode-supported cells with LSCF-SDC cathodes infiltrated with 7.6 wt% BaCO<sub>3</sub>. The cell gave an initial peak power density of 1.29, 1.08, 0.81, and 0.61 W cm<sup>-2</sup> at 800, 750, 700, and 650 °C, respectively. Figure 9b compares the single-cell performance at 700 °C. A loading of 9.2 wt% BaCO<sub>3</sub> deposited into the LSCF cathode resulted in an increase in the peak power density from 0.66 to 0.73 W cm<sup>-2</sup>, whereas it increased from 0.71 to 0.81 W cm<sup>-2</sup> when the LSCF-SDC cathode was infiltrated with 7.6 wt% BaCO<sub>3</sub>. As shown in Figure 9c, the peak power density goes through an increase when the cathodes are infiltrated with BaCO<sub>3</sub>. Because the anode and electrolyte are basically the same due to an identical fabrication process, the improvement in power density must be caused by the increased catalytic activity as a result of BaCO<sub>3</sub> deposition. It is noted that the cell with the LSCF-BaCO<sub>3</sub> cathode shows a power density that is even larger than the cell with a bare LSCF-SDC electrode. Prior observations indicate that LSCF-SDC usually shows much high electrochemical performance due to the enlarged TPB length caused by the high ionic conductivity of SDC. In addition, the active oxygen ion vacancy in SDC could enhance the surface exchange process, that is, the oxygen incorporation reaction. However, BaCO<sub>3</sub> can neither extend the reaction site nor offer additional oxygen ion vacancies because it is not an ionic conductor. Accordingly, the performance improvement should be caused by the synergistic catalytic activity of BaCO<sub>3</sub> particles.

To reveal the electrode stability, single cells with LSCF electrodes were run at a constant cell voltage of 0.7 V at 700 °C for about 340 h and the current density was recorded as a function of time, as shown in Figure 10. Initially, degradation was observed for the bare LSCF cathode as the current density went through a 15% decrease and dropped from 0.73 to 0.62 A cm<sup>-2</sup>. The degradation of single cells with bare LSCF electrodes has been widely reported by other researchers.<sup>[14,17,18]</sup> In contrast, for the cell with a BaCO<sub>3</sub>-infiltrated LSCF cathode, the current density increased slightly in the first few hours from 0.84 to 0.93 A cm<sup>-2</sup>, decreased slightly after about 50 h, and then became stable until the end of the test. After testing for 340 h, the current density of the cell with BaCO<sub>3</sub> nanoparticles was ~0.88 A cm<sup>-2</sup>, which is 0.26 A cm<sup>-2</sup> higher than that of the cell without BaCO<sub>3</sub>, which demonstrates

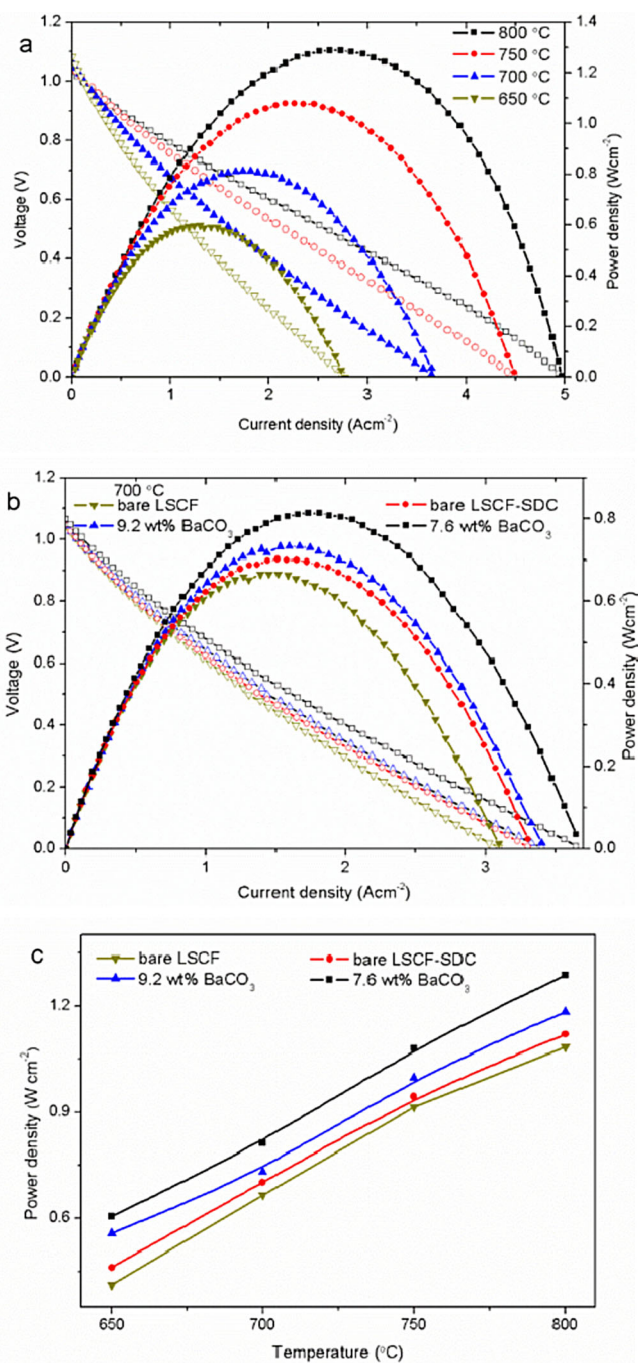


**Figure 9.** a) Cell voltages and power densities as a function of current density for a single cell with a LSCF-SDC cathode infiltrated with 7.6 wt% BaCO<sub>3</sub>, measured by using humidified hydrogen as the fuel and ambient air as the oxidant. b) The performance at 700 °C and c) a summary of peak power density for cells with different cathodes.

a 40% performance enhancement with concomitant long-term stability.

The morphology of the BaCO<sub>3</sub>-infiltrated LSCF cathode before and after the stability test was examined by using SEM and TEM (Figure 11). It was observed that the microstructures remain similar before and after operating for 340 h at 700 °C, and no obvious change in the LSCF grains was observed. In addition, the BaCO<sub>3</sub> nanoparticles maintained their size and

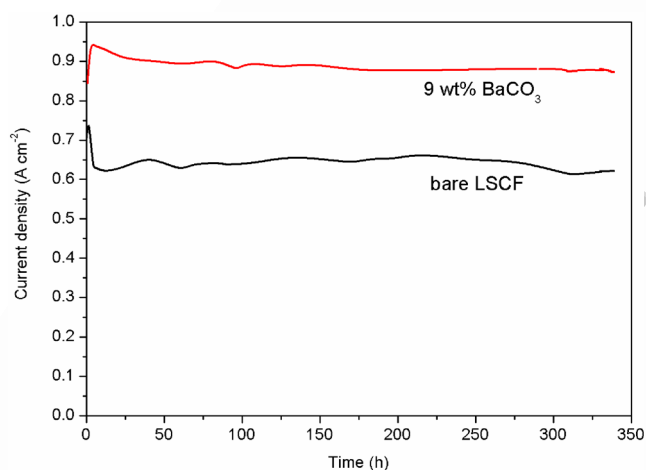


**Figure 10.** Long-term stability of anode-supported single cells with a bare LSCF cathode and a 9.2 wt% BaCO<sub>3</sub>-infiltrated LSCF cathode operated at a constant potential of 0.7 V at 700 °C for 340 h.

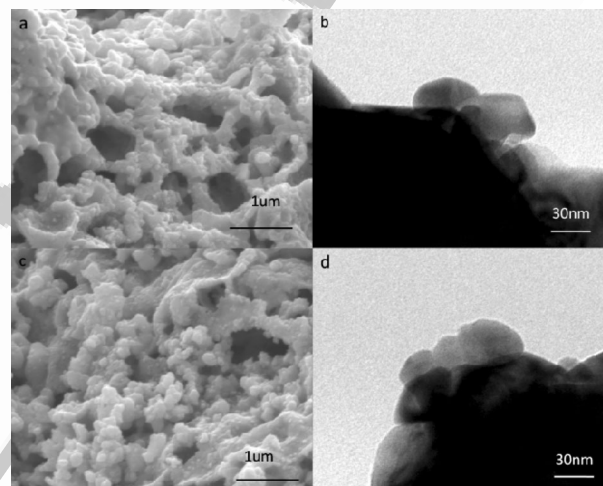


**Figure 11.** Microstructure evolution of LSCF electrodes loaded with 9 wt% BaCO<sub>3</sub> nanoparticles. SEM images of LSCF electrode morphology and TEM pictures of a BaCO<sub>3</sub> nanoparticle: a, b) fresh sample and c, d) after testing for 340 h.

shape. The unchanged microstructure suggests stable electrochemical performance, which was shown in Figure 10.

### 3. Conclusion

BaCO<sub>3</sub> nanoparticles were deposited on LSCF and LSCF-SDC electrodes as synergistic electrocatalysts for the ORR. The synergistic catalytic activity was demonstrated by the improved electrochemical performance of both LSCF and LSCF-SDC electrodes with infiltrated nanoscale BaCO<sub>3</sub> particles. These particles significantly reduced the low-frequency resistance that is associated with the surface reaction process. In addition, the particles improved the chemical oxygen surface exchange coefficients by a factor of up to eight, which demonstrates a significant enhancement in the kinetics of the surface reaction process. As a result, the particles can reduce the interfacial po-

larization resistance of both LSCF and LSCF-SDC electrodes, with an improving factor in the range of 2.37 to 3.74. Furthermore, the particles can improve the electrochemical performance of single cells with LSCF and LSCF-SDC composite cathodes, which leads to an approximately 40% improvement in peak power density and stable cell operation for over 340 h.

## Experimental Section

### Powder Preparation

LSCF ( $\text{La}_{0.6}\text{Sr}_{0.4}\text{Co}_{0.2}\text{Fe}_{0.8}\text{O}_{3-\delta}$ ) powder was prepared by using an EDTA–citric acid combustion method.<sup>[23]</sup> Stoichiometric amounts of the precursors  $\text{La}(\text{NO}_3)_3$ ,  $\text{Sr}(\text{NO}_3)_2$ ,  $\text{Co}(\text{NO}_3)_2$ , and  $\text{Fe}(\text{NO}_3)_3$  (99.5%, Sinopharm Chemical Reagent Co.) were dissolved in distilled water. Citric acid and EDTA were used in a molar ratio of 1:1:1 metal cation/citric acid/EDTA to assist the combustion process. The precursor solution was subsequently heated on a hotplate until self-combustion occurred. The resulting ashes were collected and calcined at 800 °C for 2 h to remove possible organic residues and to form the desired perovskite structure. SDC ( $\text{Sm}_{0.2}\text{Ce}_{0.8}\text{O}_{2-\delta}$ ) powder was synthesized by using a chemical coprecipitation process.<sup>[24]</sup> Cerium and samarium nitrates ( $\text{Ce}(\text{NO}_3)_3$ , 99.5%,  $\text{Sm}(\text{NO}_3)_3$ , 99%; Sinopharm Chemical Reagent Co.) were used as the cation source and ammonia carbonate ( $(\text{NH}_4)_2\text{CO}_3$ , 99%; Sinopharm Chemical Reagent Co.) was used as the precipitant. The cerium–samarium nitrate solution had a cation concentration of 0.1 mol L<sup>-1</sup> with a molar ratio of 4:1 Ce<sup>3+</sup>/Sm<sup>3+</sup>. The nitrate solution was added dropwise to a solution of ammonium carbonate (0.1 mol L<sup>-1</sup>) under mild stirring to form white carbonate precipitates at RT. The precipitates were washed three times with distilled water and subsequently rinsed with ethanol. The precursor was dried at 70 °C for 48 h, and then calcined at 600 °C for 2 h to obtain SDC powders with a single fluorite structure. YSZ ( $\text{Y}_{0.15}\text{Zr}_{0.85}\text{O}_{2-\delta}$ ) and NiO were prepared by using the glycine–nitrate process and formed by firing the ashes at 850 °C for 2 h.<sup>[25]</sup>

### Cell Fabrication

To evaluate the interfacial polarization resistance, symmetric cells with two identical LSCF and LSCF-SDC (mass ratio 6:4) cathodes were fabricated on both sides of the SDC electrolytes. Dense cylindrical SDC pellets were prepared by uniaxially pressing the SDC powders, followed by sintering at 1350 °C for 5 h. LSCF and LSCF-SDC slurries were prepared by mixing the LSCF and LSCF-SDC powders with an organic binder ( $\alpha$ -terpineol as the solvent and ethyl cellulose as the binder). The as-prepared slurry was printed onto both sides of the SDC pellets. After drying under an infrared lamp, the structure was heated at 1000 °C for 2 h to form symmetric cells. To conduct the infiltration process, appropriate amounts of barium acetate ( $\text{Ba}(\text{Ac})_2$ , 99%; Sinopharm Chemical Reagent Co.) were dissolved in water and ethanol to form a solution (0.3 mol L<sup>-1</sup>). The infiltration was carried out by placing a drop of solution on the top of the LSCF and LSCF-SDC cathode structures, letting the solution soak into the porous backbones, drying, and firing the sample at 800 °C in air for 1 h to form the  $\text{BaCO}_3$  nanoparticle catalyst. The mass of the sample before and after each infiltration treatment was measured by using an electronic balance (Mettler Toledo AB135-S) to estimate the  $\text{BaCO}_3$  loading, which was expressed as the mass ratio of  $\text{BaCO}_3$  to LSCF and LSCF-SDC.

The electrochemical performance was also characterized in anode-supported button cells that consisted of Ni-YSZ anodes, YSZ elec-

trolytes, a SDC interlayer, and LSCF-based cathodes. Solution infiltration was performed prior to testing. To fabricate the anode-supported button cells, a NiO-YSZ anode support ( $\approx 800 \mu\text{m}$ ) was first fabricated and calcined at 800 °C for 2 h. The YSZ electrolyte layer ( $\approx 10 \mu\text{m}$ ) and SDC interlayer ( $\approx 10 \mu\text{m}$ ) were sequentially deposited on the anode support by using a particle suspension coating process,<sup>[26]</sup> followed by sintering at 1400 and 1200 °C for 5 h respectively. The LSCF and LSCF-SDC cathodes were then applied by using the same procedures employed for the fabrication of symmetric cells as described above.

### Characterization of Phase Composition and Microstructure of Cathodes

X-ray diffraction (Rigaku TTR-III) analysis was used to examine the phase purity of the LSCF powders and the chemical compatibility between  $\text{BaCO}_3$  and LSCF. The microstructure and morphology of the  $\text{BaCO}_3$ -infiltrated LSCF cathodes were examined by using a scanning electron microscope (SEM, JEOL 1530) and transition electron microscope (TEM, JEOL JSM-6100).

### Electrochemical Measurements

The electrochemical performance of the cathodes was measured by using the symmetric-cells configuration with Ag as the current collector. Impedance spectra were acquired by using a Zahner Im6e electrochemical workstation with an AC amplitude of 10 mV in the frequency range of 1 MHz to 0.1 Hz. AC impedance plots were fitted by using Zview software according to the equivalent circuit with a standard deviation below 5%. The single cells were measured with humidified hydrogen (3 vol%  $\text{H}_2\text{O}$ ) as the fuel and ambient air as the oxidant. The single cell was sealed onto an alumina tube by using Ag paste (SRISR DAD-87).

### Electrical Conductivity Relaxation (ECR) Measurements

To conduct ECR measurements, the LSCF powders were ground, pressed into rectangular bars at 300 MPa, and sintered at 1400 °C for 5 h in air to form dense LSCF samples. The sintered bars had dimensions of 40.00 × 5.42 × 0.90 mm<sup>3</sup>. All sintered samples were confirmed to possess a density in excess of 95% of the theoretical density, as determined by using the Archimedes method. The average relative density was 97%. The  $\text{Ba}(\text{Ac})_2$  solution was dropped onto the bar surfaces and then heated at 800 °C to form  $\text{BaCO}_3$  particles. The conductivity of LSCF bars used for the ECR test was measured by using a standard four-probe method in a measurement system that consisted of a digital multimeter (Keithley 2001) interfaced with a computer and a program written by using the LABVIEW 8.5 software. The atmosphere changed from  $P_{\text{O}_2} = 0.01 \text{ bar}$  ( $\text{O}_2 + \text{N}_2$ ) to  $P_{\text{O}_2} = 0.1 \text{ bar}$  ( $\text{O}_2 + \text{N}_2$ ) and the total gas flow rate was maintained at 200 mL min<sup>-1</sup> to ensure that the  $P_{\text{O}_2}$  of the gas achieved equilibrium in no more than 20 s.

### Acknowledgements

We gratefully acknowledge financial support from the Collaborative Innovation Center of Suzhou Nano Science and Technology, the Ministry of Science and Technology of China (2012CB215403), and support from the Department of Energy, Nuclear Energy Research Program (DOE-NEUP) Project 14-6357, A New Paradigm

for Understanding Multi-Phase Ceramic Waste Form Performance.

**Keywords:** barium · cathode reaction · fuel cells · oxygen reduction reaction · synergistic catalysts

- [1] S. Jiang, *Solid State Ionics* **2002**, *146*, 1–22.  
 [2] E. Perry Murray, M. Sever, S. Barnett, *Solid State Ionics* **2002**, *148*, 27–34.  
 [3] D. Ding, X. Li, S. Y. Lai, K. Gerdes, M. Liu, *Energy Environ. Sci.* **2014**, *7*, 552–575.  
 [4] T. Z. Sholklipper, H. Kurokawa, C. Jacobson, S. Visco, L. De Jonghe, *Nano Lett.* **2007**, *7*, 2136–2141.  
 [5] S. P. Jiang, *Int. J. Hydrogen Energy* **2012**, *37*, 449–470.  
 [6] M. Sahibzada, S. Benson, R. Rudkin, J. Kilner, *Solid State Ionics* **1998**, *113*, 285–290.  
 [7] Y. Sakito, A. Hirano, N. Imanishi, Y. Takeda, O. Yamamoto, Y. Liu, *J. Power Sources* **2008**, *182*, 476–481.  
 [8] J. Chen, F. Liang, B. Chi, J. Pu, S. P. Jiang, L. Jian, *J. Power Sources* **2009**, *194*, 275–280.  
 [9] J. M. Serra, H.-P. Buchkremer, *J. Power Sources* **2007**, *172*, 768–774.  
 [10] Y. Liu, M. Mori, Y. Funahashi, Y. Fujishiro, A. Hirano, *Electrochem. Commun.* **2007**, *9*, 1918–1923.  
 [11] R. Jiménez, T. Klöidt, M. Kleitz, *J. Electrochem. Soc.* **1997**, *144*, 582–585.  
 [12] M. Gödickemeier, K. Sasaki, L. Gauckler, I. Riess, *J. Electrochem. Soc.* **1997**, *144*, 1635–1646.  
 [13] F. Liang, J. Chen, J. Cheng, S. P. Jiang, T. He, J. Pu, J. Li, *Electrochem. Commun.* **2008**, *10*, 42–46.  
 [14] L. Nie, M. Liu, Y. Zhang, M. Liu, *J. Power Sources* **2010**, *195*, 4704–4708.  
 [15] T. Hong, L. Zhang, F. Chen, C. Xia, *J. Power Sources* **2012**, *218*, 254–260.  
 [16] B. Hu, Y. Wang, C. Xia, *J. Power Sources* **2014**, *269*, 180–188.  
 [17] M. Liu, D. Ding, K. Blinn, X. Li, L. Nie, M. Liu, *Int. J. Hydrogen Energy* **2012**, *37*, 8613–8620.  
 [18] M. E. Lynch, L. Yang, W. Qin, J.-J. Choi, M. Liu, K. Blinn, M. Liu, *Energy Environ. Sci.* **2011**, *4*, 2249–2258.

- [19] D. Ding, M. Liu, Z. Liu, X. Li, K. Blinn, X. Zhu, M. Liu, *Adv. Energy Mater.* **2013**, *3*, 1149–1154.  
 [20] X. Lou, S. Wang, Z. Liu, L. Yang, M. Liu, *Solid State Ionics* **2009**, *180*, 1285–1289.  
 [21] T. Hong, F. Chen, C. Xia, *J. Power Sources* **2015**, *278*, 741–750.  
 [22] T. Hong, F. Chen, C. Xia, *Electrochem. Commun.* **2015**, *51*, 93–97.  
 [23] J. Martynczuk, M. Arnold, H. Wang, J. Caro, A. Feldhoff, *Adv. Mater.* **2007**, *19*, 2134–2140.  
 [24] D. Ding, B. Liu, Z. Zhu, S. Zhou, C. Xia, *Solid State Ionics* **2008**, *179*, 896–899.  
 [25] Q. Wang, R. Peng, C. Xia, W. Zhu, H. Wang, *Ceram. Int.* **2008**, *34*, 1773–1778.  
 [26] M. Liu, D. Dong, R. Peng, J. Gao, J. Diwu, X. Liu, G. Meng, *J. Power Sources* **2008**, *180*, 215–220.  
 [27] N. Grunbaum, L. Dessemond, J. Fouletier, F. Prado, L. Mogni, A. Caneiro, *Solid State Ionics* **2009**, *180*, 1448–1452.  
 [28] Y. Wang, L. Zhang, F. Chen, C. Xia, *Int. J. Hydrogen Energy* **2012**, *37*, 2182–2186.  
 [29] F. S. Baumann, J. Fleig, M. Konuma, U. Starke, H.-U. Habermeier, J. Maier, *J. Electrochem. Soc.* **2005**, *152*, A2074–A2079.  
 [30] F. S. Baumann, J. Fleig, H.-U. Habermeier, J. Maier, *Solid State Ionics* **2006**, *177*, 1071–1081.  
 [31] J.-W. Lee, Z. Liu, L. Yang, H. Abernathy, S.-H. Choi, H.-E. Kim, M. Liu, *J. Power Sources* **2009**, *190*, 307–310.  
 [32] L. Zhang, Y. Liu, Y. Zhang, G. Xiao, F. Chen, C. Xia, *Electrochem. Commun.* **2011**, *13*, 711–713.  
 [33] Y. Wang, L. Zhang, C. Xia, *Int. J. Hydrogen Energy* **2012**, *37*, 8582–8591.  
 [34] H. Bouwmeester, M. Den Otter, B. Boukamp, *J. Solid State Electrochem.* **2004**, *8*, 599–605.  
 [35] B. Hu, Y. Wang, C. Xia, *J. Electrochem. Soc.* **2015**, *162*, F33–F39.

Manuscript received: December 8, 2015

Accepted Article published: January 28, 2016

Final Article published: ■■■■, 2016

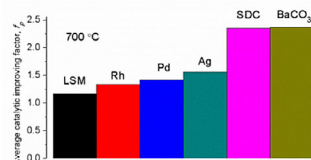
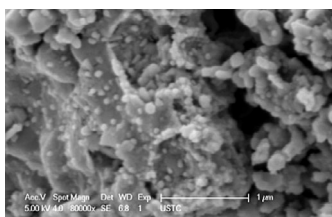
# ARTICLES

T. Hong, K. S. Brinkman, C. Xia\*

■■■ - ■■■

## Barium Carbonate Nanoparticles as Synergistic Catalysts for the Oxygen Reduction Reaction on

### $\text{La}_{0.6}\text{Sr}_{0.4}\text{Co}_{0.2}\text{Fe}_{0.8}\text{O}_{3-\delta}$ Solid-Oxide Fuel Cell Cathodes



## Barium carbonate nanoparticles:

BaCO<sub>3</sub> nanoparticles are applied in solid-oxide fuel cell cathodes by using an infiltration method to enhance the oxygen reduction reaction. The performance-improving factor of BaCO<sub>3</sub> is larger than  $\text{La}_{0.8}\text{Sr}_{0.2}\text{MnO}_{3-\delta}$  (LSM), Rh, Pd and Ag, even reaching the same level as  $\text{Sm}_{0.2}\text{Ce}_{0.8}\text{O}_{1.9}$  (SDC; see figure).



Synergistic #catalysts for #oxygenreductionreaction in solid-oxide #fuelcells @ClemsonUniv **SPACE RESERVED**  
FOR IMAGE AND LINK

Share your work on social media! *ChemElectroChem* has added Twitter as a means to promote your article. Twitter is an online microblogging service that enables its users to send and read text-based messages of up to 140 characters, known as “tweets”. Please check the pre-written tweet in the galley proofs for accuracy. Should you or your institute have a Twitter account, please let us know the appropriate username (i.e., @accountname), and we will do our best to include this information in the tweet. This tweet will be posted to the journal’s Twitter account @ChemElectroChem (follow us!) upon online publication of your article, and we recommended you to repost (“retweet”) it to alert other researchers about your publication.

Please check that the ORCID identifiers listed below are correct. We encourage all authors to provide an ORCID identifier for each coauthor. ORCID is a registry that provides researchers with a unique digital identifier. Some funding agencies recommend or even require the inclusion of ORCID IDs in all published articles, and authors should consult their funding agency guidelines for details. Registration is easy and free; for further information, see <http://orcid.org/>.

Dr. Tao Hong  
Dr. Kyle S. Brinkman  
Dr. Changrong Xia